IEEE TRANSACTIONS ON
PLASMA
SCIENCE

IEEE Xplore® Digital Library
http://ieeexplore.ieee.org/Xplore

Inverse liner Z-pinch: An experimental pulsed power platform for studying radiative shocks

T. Clayson*‡, S.V. Lebedev*, F. Suzuki-Vidal*, G.C. Burdiak*‡, J.W.D. Halliday*, J.D. Hare*, J. Ma†, L.G. Suttle*, E.R. Tubman*

*Blackett Laboratory, Imperial College, London, SW7 2AZ, United Kingdom

†Northwest Institute of Nuclear Technology, Xian 710024, China

‡Current address: First Light Fusion Ltd, OX5 1QU, United Kingdom

***Abstract*—We present a new experimental platform for studying radiative shocks using an "inverse liner z-pinch" configuration. This platform was tested on the MAGPIE pulsed power facility ($\sim$1 MA with a rise time of $\sim$240 ns) at Imperial College London in the UK. Current is discharged through a thin-walled metal tube (a liner) embedded in a low density gas-fill and returned through a central post. The resulting magnetic pressure inside the liner launched a cylindrically symmetric, expanding radiative shock into the gas-fill at $\sim$10 km/s. This experimental platform provides good diagnostic access, allowing multi-frame optical self-emission imaging, laser interferometry and optical emission spectrography to be fielded. Results from experiments with an Argon gas-fill initially at 0.04 mg/cm^3 are presented, demonstrating the successful production of cylindrically symmetric, expanding shocks which exhibit radiative effects such as the formation of a radiative precursor.**

***Index Terms*—radiative shocks, pulsed power**

I. Introduction

Radiative effects occur in high Mach number shocks when the radiative flux from thermal emission of the hot post shock material is non-negligible, resulting in significant changes to the shock structure and the formation of a radiative shock [1], [2]. Understanding these phenomena is of great importance to the High Energy Density Physics (HEDP) community due to their presence in inertial confinement fusion implosions [3] and their abundance in astrophysical events [4].

Radiation emitted by the post-shock material results in radiative cooling and thus an increase in post-shock compression (exceeding the maximum compression in a non-radiating shock of $\times 4$ for an adiabatic index of $5/3$) [1], [2], [5]. In some cases this could lead to the onset of instabilities such as the Vishniac thin-shell over-stability [6]–[8]. In addition, material ahead of the shock front is able to reabsorb this radiation, resulting in photoionization and heating of the pre-shock material. This manifests itself as a radiative precursor, a layer of heated and ionized gas ahead of the shock front [2].

It is possible to produce radiative shocks in laboratory experiments using lasers focused onto a pin embedded in a gas [9], a cluster gas [10]–[12] or a piston attached to a gas cell [13]–[21]. Radiative shocks have also been produced on pulsed power generators using imploding liners with an internal gas fill [22]–[24]. In these experiments $\sim$1 MA of current was discharged through a gas filled liner (a thin-walled metal tube). The liner did not move on the time scales of the experiment and instead multiple cylindrically converging radiative shocks were observed launched into a low density gas that filled the liner. These shocks exhibited radiative effects such as the formation of a radiative precursor. However, the limited radius of the liners (3 mm) prevented the shocks evolving unimpeded, with the radiative precursor extending over a similar length scale.

This paper introduces a new experimental platform for studying radiative shocks which was demonstrated on the MAGPIE pulsed power facility ($\sim$1 MA with a rise time of in $\sim$240 ns) [25] at Imperial College London in the UK. This platform uses an "inverse liner z-pinch" setup to produce cylindrically expanding radiative shocks which are able to propagate unimpeded for several microseconds over a distance of 50 mm. The experimental results presented here show that the radiative shocks are reproducible and initially uniformity, allowing this platform to be used for benchmarking numerical radiative-hydrodynamic simulations, and studying radiative instabilities.

II. Experimental setup

The experimental platform for the inverse liner z-pinch setup is Fig 1. A 3D diagram depicting how the shocks are driven is shown in Fig 1.a. The $\sim$1 MA current of the MAGPIE generator [25] was discharged through a 20 mm long stainless steel liner with an inner diameter of 11 mm and wall thickness of 100 μm. Current was then returned through a 5 mm diameter cylindrical electrode on the axis, generating a toroidal magnetic field with a peak of $\sim$40 T on the inner surface of the liner. The resulting magnetic pressure of $\sim$400 MPa resulted in a cylindrically symmetric, radially expanding shock, propagating at $\sim$10 km/s, being launched in to an Argon gas-fill initially at 0.04 mg/cm^3. The liner did not move on the time scale of the experiment and did not melt. A 3D cutaway of a CAD model is shown in Fig 1.b, with all dimensions in millimetres, and a photo of the liner in the MAGPIE chamber is shown in Fig 1.c.

The MAGPIE transfer line delivering current to the liner is kept under vacuum and so a uniform gas-fill around the liner was provided by a separate gas-cell, shown in the 3D cutaway in Fig 1.d. This gas cell provided a large volume with an internal radius of 66.5 mm and height of 33 mm, allowing shocks to evolve unimpeded for several microseconds. The

Digital Object Identifier: 10.1109/TPS.2018.2868757

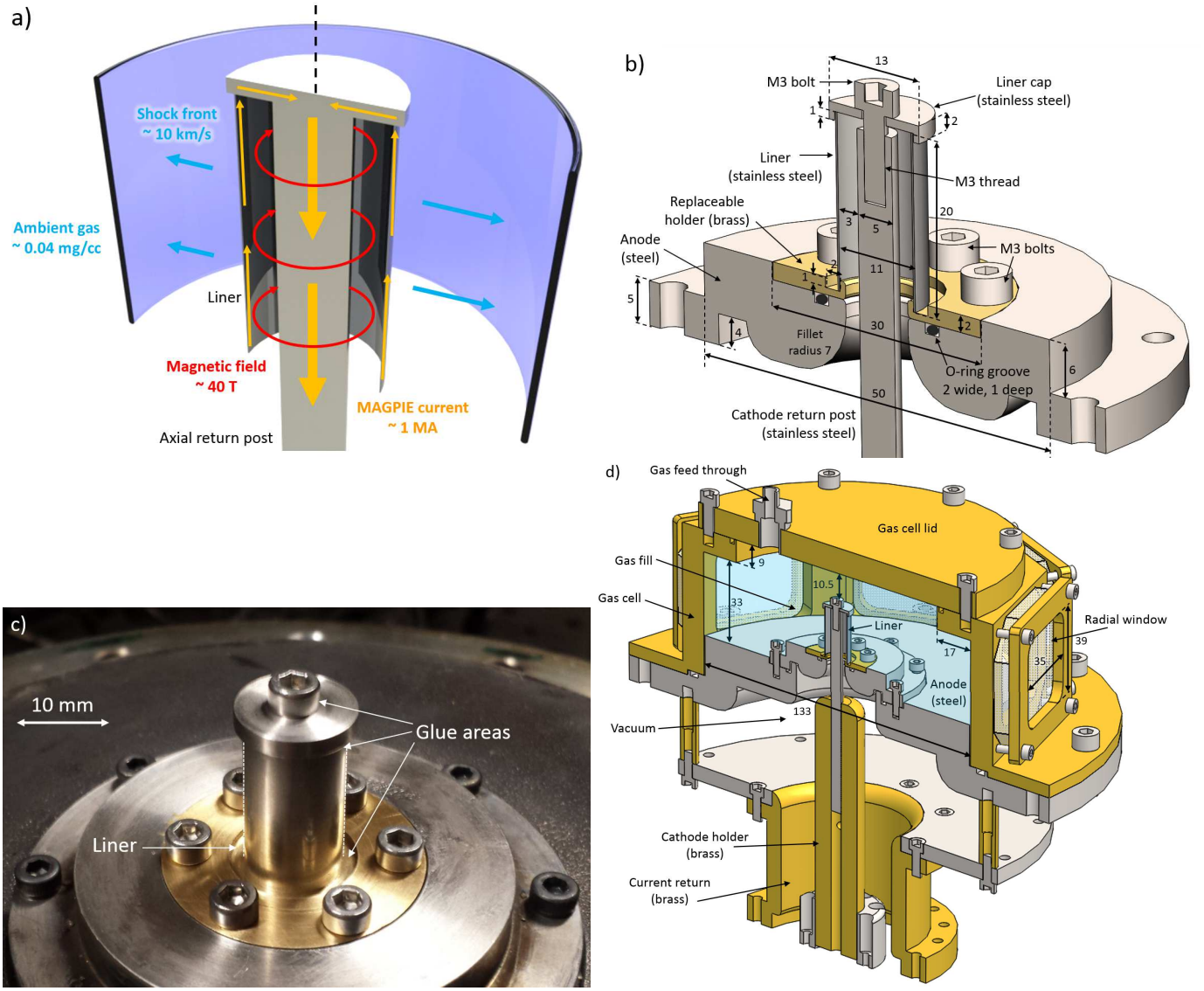

Fig. 1. (a) 3D Diagram of the "inverse liner" experimental setup highlighting the current path in yellow, toroidal magnetic field in red and radially expanding shock in blue. (b) 3D cutaway of a CAD model, dimensions in millimeters. (c) Photo of the liner in the MAGPIE experimental chamber. (d) 3D cutaway of a CAD model of the experimental hardware and gas cell, dimensions in millimeters.

gas cell exterior was octagonally shaped allowing for eight radially facing windows, each with a height of 35 mm and width of 39 mm, providing side on diagnostic access to the experiment.

The short distance between the liner and the axial electrode (3 mm) required the interior of the liner to also be under vacuum to prevent electrical breakdown, and so the liner formed part of the gas seal. To create a gas tight seal between the liner and the rest of the hardware, clamps and rubber O-rings were used. However, these reduced the effective liner length to $\sim$11 mm and also drove large edge effects. Later experiments instead used a coating of Araldite Instant [26] (a two component epoxy adhesive which begins setting in 90 seconds) around the joints between the liner and hardware, which reduced the magnitude of these edge effects and increased the effective liner length.

The diagnostic setup is depicted in Fig 2. All diagnostics were imaged along the same line of sight, allowing for direct comparisons. A Mach-Zehnder laser interferometer was fielded to measure the electron density both ahead and behind the shock. The second harmonic of an SBS compressed, pulsed Nd-YAG laser (EKSPLA SL321P) was used to produce a $\sim$0.5 ps pulse with a wavelength of 532 nm which was then recorded with a commercial Canon DSLR with an exposure greater than the experiment duration. Optical self-emission from the plasma was recorded with a high-speed, multiframe camera (Invisible Vision U2V1224) on twelve images with exposures of 10 ns and an interframe time of 40 ns. A low pass filter was inserted in front of this camera to block the laser light and so this diagnostic was sensitive to wavelengths $>$ 600 nm. In addition,

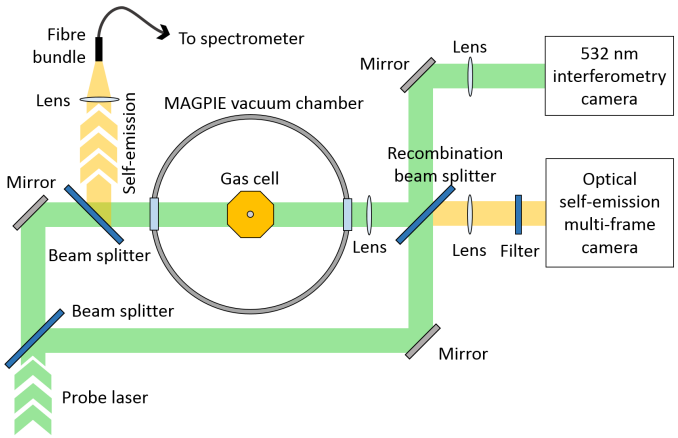

Fig. 2. Top down diagram showing the diagnostic setup. Laser interferometry, self-emission multiframe and optical spectroscopy were all performed along the same line of sight.

a bundle of fourteen optical fibres imaged the plasma self-emission from $\sim$250 μm diameter collection volumes spaced 580 μm apart, radially away from the liner surface. These were imaged onto an ANDOR SR-500i-A spectrometer with a 400 lines/mm grating and exposure of 8 ns, recording spectra between between $435-490$ nm.

III. Experimental results

A time sequence of current through the liner and timings of diagnostics are shown for two similar experiments, with the same Argon gas-fill initially at 0.04 mg/cm^3, in Fig 3. Current was determined with two Rogowski coils and increased current was found to result in slightly increased shock velocities, with $\sim$13 km/s measured for Fig 3.a with a peak current of $\sim$1.2 MA and 10 km/s measured for Fig 3.b with a peak current of $\sim$1.1 MA.

A. Optical self-emission

The evolution of the radiative shocks was studied with the multiframe camera which recorded twelve images from a single experiment. A selection of images from a typical experiment (that shown in Fig 3.a) are shown in Fig 4.a. The liner can be seen as the dark region in the centre, labelled in the top image. Although 20 mm long in total, this experiment used the initial design with O-ring clamps which reduced the effective liner length to $\sim$11 mm. The shock can be seen as bright emission to the left and right of the liner, labelled in the second image, propagating radially outwards from the liner surface.

Additional shocks were launched from the top and bottom of the liner due to interaction with the surrounding hardware, labeled as 'edge shocks' in the bottom image. All measurements were therefore made along the mid height of the liner where the primary radial shock remained uniform.

To measure the shock velocity, a horizontal lineout was taken at a height of 5 mm (shown in the third image of Fig 4.a) averaged vertically over 200 μm. In each lineout

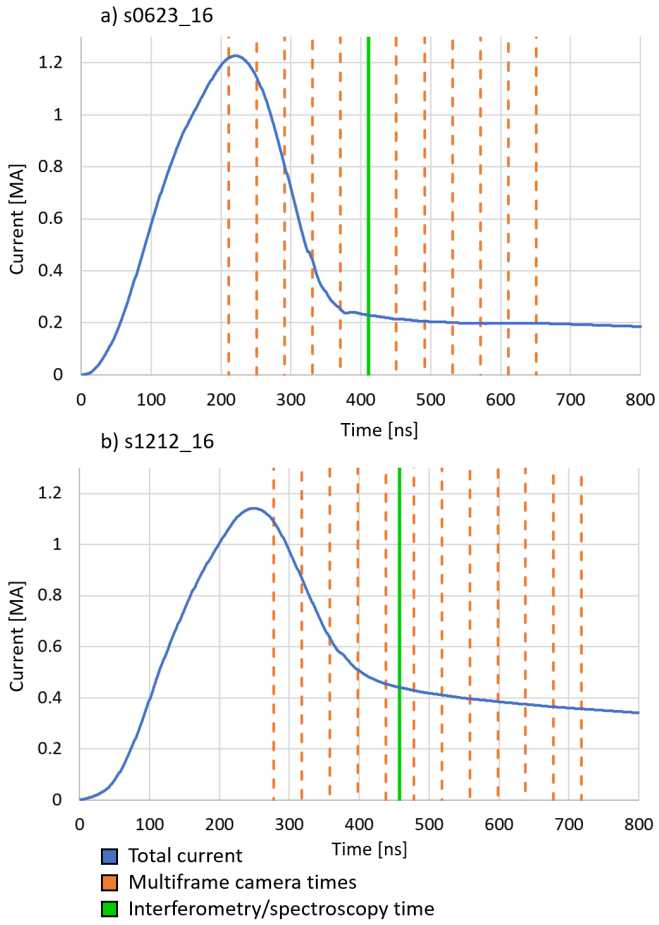

Fig. 3. Current through the liner as a function of time for two identical experiments. Timings of different diagnostics are indicated.

the shock front position was then identified as the rising edge in the intensity profile. Measurements from both the left and right side of Fig 4.a are plotted as a function of time after current start in Fig 4.b. Error bars have been set to the minimum resolution of the multiframe camera at which features may be resolved, measured to be $\sim$630 μm (motion blurring due to the velocity of the shock is expected to be of the order of 100 μm). Positions from both the left and right shock follow a near identical trajectory indicating that current was discharged uniformly through the liner resulting in cylindrically symmetric expanding shocks. These points closely follow a linear trendline indicating that shock velocity remains constant over the observed time, $\sim$500 ns.

Measurements from fourteen separate experiments indicate shocks propagated at a constant velocity between $7-13$ km/s, depending on the MAGPIE drive current. In addition, the shock launch time was determined by extrapolating trendlines to the liner surface at 5.6 mm. This yielded a launch time of 187 ± 24 ns after current start. These launch times are comparable to those seen in previous converging shock experiments [24] while velocities are slower by a factor of 2 ($\sim$10 km/s instead of $\sim$20 km/s) primarily due to the

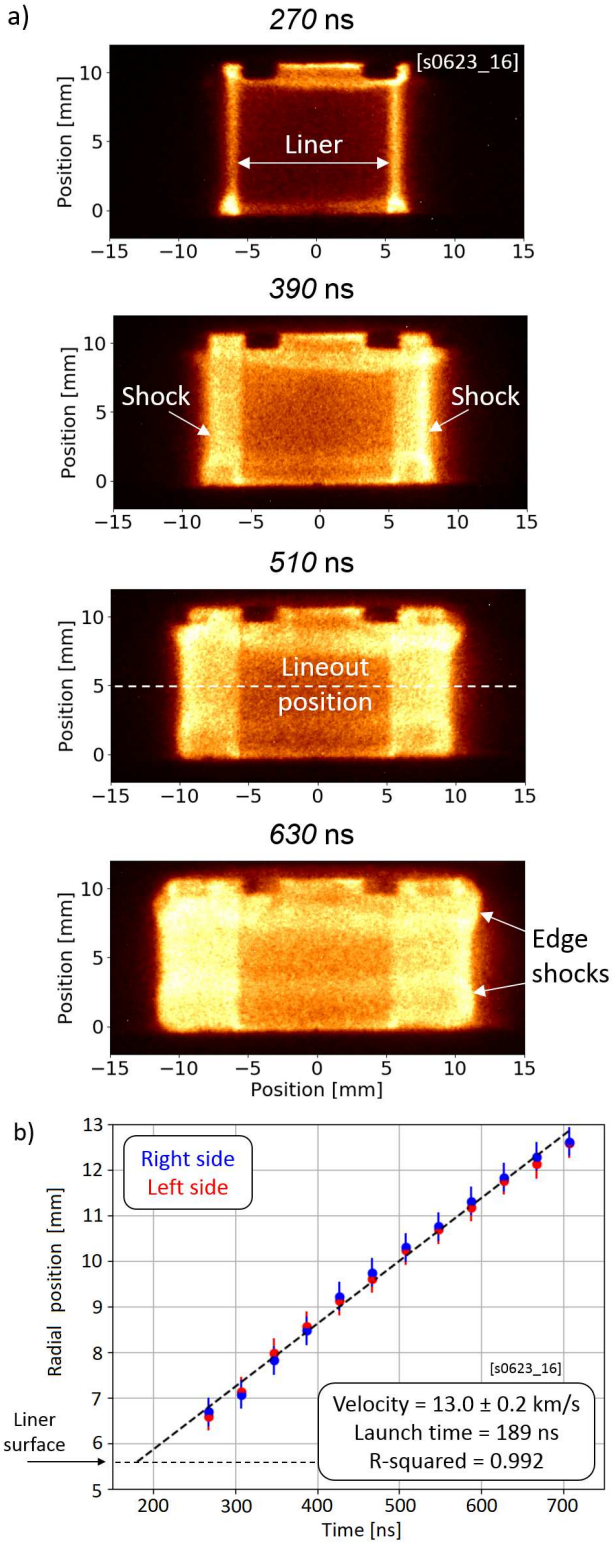

Fig. 4. (a) Optical self-emission images from the shot shown in Fig 3.a. The liner is seen as the dark region in the centre while the shocks expand radially and can be seen as regions of bright emission. (b) Shock front position plotted as a function of time. A linear trend line, shown with a dashed line closely fits the data allowing the velocity to be determined.

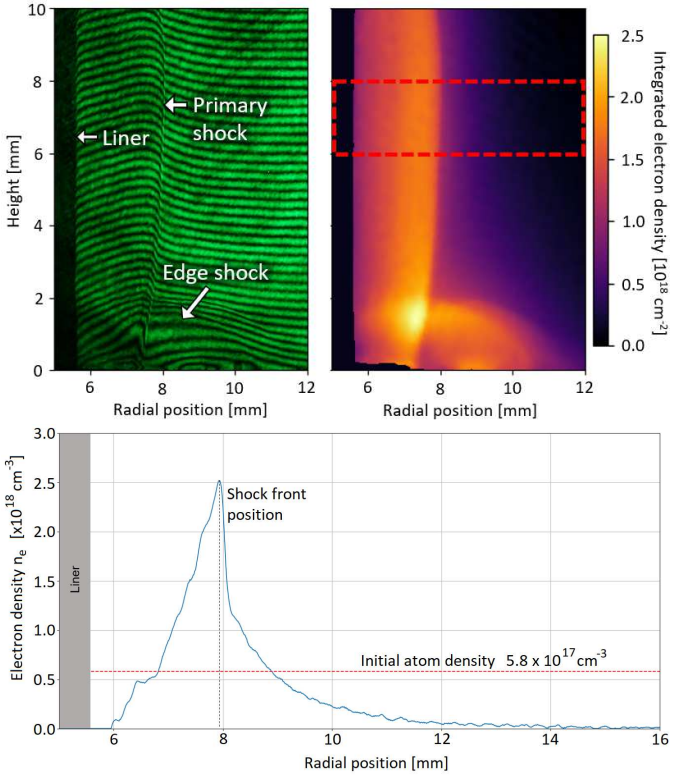

Fig. 5. (a) Interferometry image from the experiment shown in Fig 3.b taken at 460 ns. (b) processed image showing a map of electron density integrated along the probe beams path, $n_e L$. (c) A lineout taken from the hashed position marked in (b) has been Abel inverted showing electron density as a function of radius.

increased mass-density of the gas-fill. However, in contrast to the multiple shocks observed in converging shock experiments, only a single shock (ignoring edge effects) is observed in the experiments described in this paper. The larger liner diameter (11 mm instead of 6 mm) resulted in less Ohmic heating which was insufficient to melt the liner.

B. Laser interferometry

Laser interferometry records variations in refractive index of the plasma as fringe shifts in an interferogram. An example image (from the experiment shown in Fig 3.b) is shown in Fig 5.a, taken 460 ns after current start. To maximise spatial resolution the laser interferometry used a higher magnification, imaging a 12×10 mm field of view on one side of the liner. Due to cylindrical symmetry of the system this was representative of the entire radially expanding shock. The surface of the liner is visible to the left (< 5.6 mm) and the shock propagates to the right, with the shock front visible as the steep shift in fringes at ~ 8 mm.

The shift of these fringes is proportional to the electron density integrated along the path of the beam, $n_e L$, and thus these images can be used to produce 2-D maps of $n_e L$ following the procedure described in [27]. The resulting map is shown in Fig 5.b.

Edge effects are more prominent in these images and a large 'edge shock' can be seen at the base of the liner which interacts with the primary shock, resulting in regions of enhanced electron density. In addition, the primary shock bends towards the edge of the liner, slightly deviating from the approximately 1-D cylindrical expansion.

A horizontal lineout of $n_e L$ was taken through the region that most resembled a 1-D expansion, averaged between a height of 6 mm and 8 mm (indicated by the hashed area in Fig 5.b). This $n_e L$ profile was used to determine the electron density as a function of radius using an Abel inversion. The result is shown in Fig 5.c together with the initial atom density of $n_i = 5.8 \times 10^{17}$ cm^{-3} indicated with a dashed red line.

A peak electron density of 2.5×10^{18} cm^{-3} at a radial position of 7.95 mm corresponds with the shock front position. Dividing by the initial gas-fill atom density yields a peak ionization of $Z \sim 4$ for the radiative precursor. Behind the shock front the electron density rapidly decreases, suggesting the shock is similar to a blast wave with an expanding thin shell of dense material followed by hot, low density gas.

Without radiative effects, ionization ahead of the shock front would be expected to be zero. Instead the interferometry shows that electron density decays gradually over ~4 mm ahead of the shock front, indicating the unshocked material is being ionized and thus a precursor is formed. This is similar to results from converging shock experiments [22]–[24].

C. Optical spectroscopy

To obtain an independent estimate of the level of ionization in both the precursor and shocked material, optical spectroscopy was fielded on the experiment shown in Fig 3.a. Self-emission spectra between $435 - 490$ nm were recorded from fourteen points spaced radially outwards from the liner surface, three of which are shown in Fig 6.a. Spectra from the post-shock region (fibre 1), the approximate shock front position (fibre 5) and the precursor (fibre 9) are shown in Fig 6.b. For clarity of presentation the spectrum from the precursor region has been multiplied by a factor of 5.

The spectra bear remarkable similarities and the same lines are present in all spectra. However, spectra from the precursor region is significantly dimmer than that from the shock front. Persistent lines of Ar-II are present in these spectra, such as the $3s^2 3p^4 4p$ to $3s^2 3p^4 4s$ transitions at 461.0 nm and 480.6 nm. However, the lack of significant Ar-III contribution, such as the $3s^2 3p^3 4p$ to $3s^2 3p^3 3d$ transitions at 456.5 nm and 468.8 nm suggest the plasma is only singly ionized in both the post-shock and precursor regions.

To improve on this estimate, the atomic physics code PrismSPECT [28] was used to simulate the expected spectrum at various points in the radiative precursor. Simulations were run for an Argon plasma at 0.04 mg/cm^3, at a variety of temperatures, with Detailed Configuration Accounting (DCA), the Low Temperature Spectroscopy atomic model and zero width. As an initial estimate the plasma was assumed to be in steady state, which may not be accurate for the precursor region. By visually comparing the presence of lines in the calculated spectrum to that obtained in experiments the temperature was estimated to be $1.5 - 2.5$ eV (the simulated spectrum for a plasma at 2.5 eV is shown in Fig 6.c) with an average ionization of $Z = 0.5 - 1.2$ at all points in the radiative precursor and post-shock region, similar to results from converging shock experiments [23].

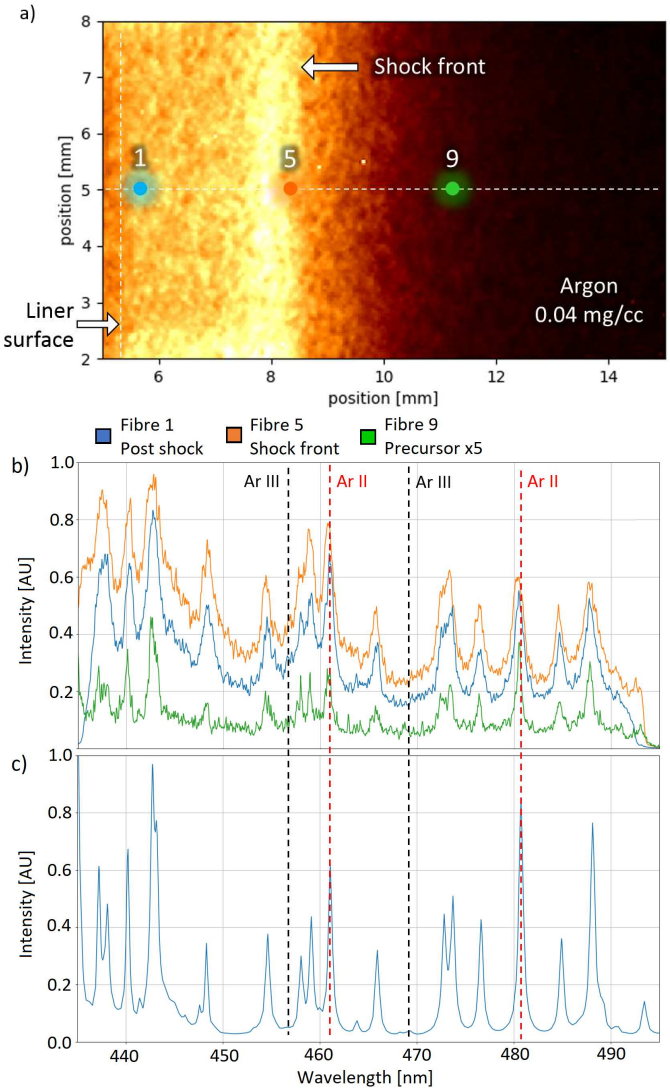

Fig. 6. (a) Focal points of several fibres superimposed on a self-emission image taken at approximately the same time. (b) Spectrum recorded from the experiment shown in Fig 3.a taken at 410 ns. (c) PrismSPECT simulated spectrum for an Argon plasma at 0.04 mg/cm^{-3} and 2.5 eV.

IV. Discussion

A. Temperature across the shock

The post-shock ion temperature, T_i may be estimated to be [2], [5]:

$$T_i = 2\frac{\gamma - 1}{k_B(\gamma + 1)^2}\frac{Am_p}{Z + 1}u_s^2 \quad (1)$$

where γ is the adiabatic index (assumed to be $\gamma = 5/3$ for a monatomic gas such as Argon), k_B is Boltzmann's constant,

A is the relative atomic mass (39.9 for Argon), m_p is the proton mass, Z is the average ionization and u_s is the shock velocity (found to be $\sim 10^4$ m/s). Assuming that the post-shock ionization is not dissimilar to the peak ionization observed in the precursor (found to be $Z \sim 4$ in Fig 7) yields a temperature of 1.6 eV, agreeing with optical spectroscopy estimates of $1.5 - 2.5$ eV.

B. Formation of the radiative precursor

The precursor observed in these experiments is expected to have formed due to reabsorption of radiation emitted by the shock front. However, precursors ahead of the shock may also form due to particles reflected by the shock front depositing their energy ahead of the shock or due to thermal conduction [2].

To determine if electron or ion acceleration plays a role, the electron and ion mean free path were calculated using [29]:

$$\lambda_e(cm) = 2 \times 10^{18} \frac{[T_e(KeV)]^2}{Z n_e(cm^{-3})} \tag{2}$$

$$\lambda_i(cm) = 2 \times 10^{18} \frac{[T_i(KeV)]^2}{Z^3 n_e(cm^{-3})} \tag{3}$$

where Te and T_i are the electron and ion temperature respectively and n_e is the electron density. Temperature and ionization estimates were taken from optical spectroscopy, assuming $T_i = T_e \sim 2$ eV and $Z \sim 0.9$. The electron density was calculated by multiplying the gas-fill initial atom density by the ionization, yielding $n_e = 4.6 \times 10^{17}$ cm^{-3}. This yielded a mean free path of $\lambda_e \sim 190$ nm and $\lambda_i \sim 240$ nm for the electron and ions respectively, both of which are significantly smaller than the observed precursor. However, to fully discount this mechanism the mean free path was recalculated for ions travelling at the shock velocity, with a kinetic energy of ~ 21 eV. This yielded a larger ion mean free path of ~ 26 μm, but still significantly smaller than the observed precursors scale and below the resolution of the laser interferometry diagnostic. Thus this mechanism may be ignored in this system.

To determine if thermal conduction was responsible for the formation of the precursor, the thermal diffusion was approximated as a Marshak wave [2] where the conductivity, k_{th}, is given by:

$$k_{th} = 2 \times 10^{21} \frac{[T_e(eV)]^{5/2}}{ln(\Lambda) Z(Z+1) n_i(cm^{-3})} C_p \rho \tag{4}$$

where $ln(\Lambda)$ is the Coulomb logarithm (assumed to be ~ 4 for these plasma conditions), C_p is the heat capacity at constant pressure ($\sim 5.2 \times 10^6$ erg/g/K for Argon [30]) and ρ is the density (in g/cm^3) of the unshocked medium. Using the previous estimates for temperature and ionization, $T_e \sim 2$ eV and $Z \sim 0.9$, yields a conductivity of $k_{th} \sim 5.9 \times 10^5$ g.cm/s^{3}K. The position of the thermal wave front, x_0, in a Marshak wave as a function of time, t, is given by [2]:

$$x_0 = \frac{\sqrt{n+2}}{n+1} \sqrt{\frac{2 k_{th}}{\rho C_V}} \sqrt{2t} \tag{5}$$

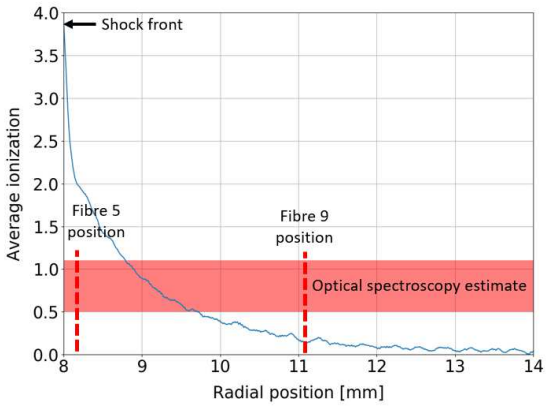

Fig. 7. Ionization in the precursor, determined by dividing the electron density shown in Fig 5 by the gas-fill initial atom density. The range of ionizations estimated from optical spectroscopy is highlighted in red and shows poor agreement with estimates from interferometry.

where n is a dimensionless number, ~ 4 in high density materials [2], and C_V is the heat capacity at constant volume. Using the electron thermal conductivity previously calculated and assuming the process is approximately adiabatic (so that $C_V = C_P/\gamma$) indicates the Marshak wave has propagated ~ 0.3 mm after ~ 200 ns (the time between the shock being launched and the interferometry image). This is insufficient to account for the large precursor observed ahead of the shock front. However, this should be resolvable by the interferometry diagnostic and may partially contribute to the precursor directly ahead of the shock front. However, this model does not take into account the motion of the shock front itself and thus is likely to be a significant overestimate.

C. LTE in the radiative precursor

Estimates of ionization throughout the precursor from interferometry were found by dividing the electron density by the initial gas-fill atom density, yielding the plot shown in Fig 6. This shows a gradually decreasing ionization while optical spectroscopy shows a similar spectrum at all regions in the precursor, suggesting a constant temperature and ionization. For example, optical spectroscopy taken ~ 3 mm ahead of the shock front, shown in the green curve in Fig 7.a, estimates an ionization of $Z = 0.5 - 1.2$ while laser interferometry estimates an electron density of $\sim n_e = 1 \times 10^{-17}$ corresponding with an average ionization of $Z \sim 0.2$. These observations match those in [23] in which it was suggested that the precursor is not in LTE and photo-ionization results in a small fraction of ions dominating the emission spectrum. To verify this, the ion collision times were estimated for different regions in the precursor using [29]:

$$\tau_i = 4 \times 10^{12} \frac{\sqrt{A} [T_i(KeV)]^{2/3}}{Z^3 n_e(cm^{-3})} \tag{6}$$

This yielded collision times of $\tau_i(r = 9 \text{ mm}) = 10$ nm, $\tau_i(r = 10 \text{ mm}) = 680$ nm and $\tau_i(r = 11 \text{ mm}) = 11$ μm. A shock with a velocity of ~ 10 km/s will propagate 1 mm

in 100 ns. Therefore the region at $r = 9$ mm ($\sim$1 mm ahead of the shock front) has sufficient time for many ion collisions and thus is expected to be approximate LTE state, while more distant regions have insufficient time to thermalize and thus are likely to be in non-LTE. This confirms conclusions suggested in [23].

V. Conclusion

A novel platform for studying radiative shocks has been demonstrated on the MAGPIE pulsed power facility ($\sim$1 MA in 240 ns) at Imperial College London in the UK. This platform is capable of producing cylindrically expanding radiative shocks which propagate at a constant velocity of $\sim$10 km/s for over 500 ns in an Argon gas-fill initially at 0.04 mg/cm^3. The formation of a radiative precursor is observed, extending $\sim$3 mm ahead of the shock front. Interferometry and optical spectroscopy were found to disagree on ionization in the radiative precursor region. This suggests that the radiative precursor is not in LTE and photo-ionization results in a small fraction of ionized ions dominating the emission spectrum. These experiments have been expanded to include a range of other gas-fills, allowing these radiative shocks to be characterised for a range of elements, to be detailed in future publications.

The uniformity and reproducibility of the radiative shocks produced with this platform makes it suitable for the study of perturbed radiative shocks and radiative instabilities. Controllable perturbations may be seeded in to the shock by carving grooves on the surface of the liner. The spacing and depth of these grooves allows the wavelength and amplitude of perturbations in the radiative shock to be controlled. This has been experimentally verified. By seeding perturbations of a specific wavelength it is hoped that this setup could be used to study radiative plasma instabilities such as the Vishniac instability [6]. This will be the subject of future publications.

Acknowledgment

This work was supported by the Engineering and Physical Sciences Research Council (EPSRC) through a DTA studentship and by the U.S. Department of Energy (DOE) Awards No. DE-F03-02NA00057 and No. DE-SC-0001063. The authors would like to acknowledge the Imperial College London Institute of Shock Physics for use of their multiframe camera.

References

[1] Y. B. Zel'dovich and Y. P. Raizer, *Physics of Shock Waves and High-Temperature Hydrodynamic Phenomena*. Dover Publications, 2002.

[2] R. P. Drake, *High Energy Density Physics: Fundamentals, Inertial Fusion, and Experimental Astrophysics*. Springer, Berlin, 2006.

[3] A. Pak, L. Divol, G. Gregori, S. Weber, J. Atherton, R. Bennedetti, D. K. Bradley, D. Callahan, D. T. Casey, E. Dewald, T. Döppner, M. J. Edwards, J. A. Frenje, S. Glenn, G. P. Grim, D. Hicks, W. W. Hsing, N. Izumi, O. S. Jones, M. G. Johnson, S. F. Khan, J. D. Kilkenny, J. L. Kline, G. A. Kyrala, J. Lindl, O. L. Landen, S. Le Pape, T. Ma, A. Macphee, B. J. Macgowan, A. J. Mackinnon, L. Masse, N. B. Meezan, J. D. Moody, R. E. Olson, J. E. Ralph, H. F. Robey, H. S. Park, B. A. Remington, J. S. Ross, R. Tommasini, R. P. J. Town, V. Smalyuk, S. H. Glenzer, and E. I. Moses, "Radiative shocks produced from spherical cryogenic implosions at the National Ignition Facility," *Physics of Plasmas*, vol. 20, no. 056315, 2013.

[4] B. A. Remington, R. P. Drake, and D. D. Ryutov, "Experimental astrophysics with high power lasers and Z pinches," *Reviews of Modern Physics*, vol. 78, no. 3, 2006.

[5] R. P. Drake, "Radiative Shocks in the Laboratory," *Astrophysics and Space Science*, vol. 298, no. 1-2, 2005.

[6] E. T. Vishniac, "The dynamic and gravitational instabilities of spherical shocks," *The Astrophysical Journal*, vol. 274, nov 1983.

[7] J. M. Laming and J. Grun, "Dynamical Overstability of Radiative Blast Waves: The Atomic Physics of Shock Stability," *Physical Review Letters*, vol. 89, no. 12, 2002.

[8] J. Grun, J. Stamper, C. Manka, J. Resnick, R. Burris, J. Crawford, and B. Ripin, "Images of unstable Taylor-Sedov blast waves propagating through a uniform gas," *Physical Review Letters*, vol. 66, no. 21, 1991.

[9] A. D. Edens, R. G. Adams, P. Rambo, L. Ruggles, I. C. Smith, J. L. Porter, and T. Ditmire, "Study of high Mach number laser driven blast waves in gases," *Physics of Plasmas*, vol. 17, no. 112104, 2010.

[10] M. J. Edwards, A. J. MacKinnon, J. Zweiback, K. Shigemori, D. Ryutov, A. M. Rubenchik, K. A. Keilty, E. Liang, B. A. Remington, and T. Ditmire, "Investigation of Ultrafast Laser-Driven Radiative Blast Waves," *Physical Review Letters*, vol. 87, no. 8, 2001.

[11] A. S. Moore, E. T. Gumbrell, J. Lazarus, M. Hohenberger, J. S. Robinson, R. A. Smith, T. J. A. Plant, D. R. Symes, and M. Dunne, "Full-trajectory diagnosis of laser-driven radiative blast waves in search of thermal plasma instabilities," *Physical Review Letters*, vol. 100, no. 055001, 2008.

[12] M. Hohenberger, D. Symes, J. Lazarus, H. Doyle, R. Carley, A. S. Moore, E. Gumbrell, M. Notley, R. Clarke, M. Dunne, and R. Smith, "Observation of a Velocity Domain Cooling Instability in a Radiative Shock," *Physical Review Letters*, vol. 105, no. 205003, 2010.

[13] T. Clayson, F. Suzuki-Vidal, S. V. Lebedev, G. Swadling, C. Stehle, G. C. Burdiak, J. M. Foster, J. Skidmore, P. Graham, E. Gumbrell, S. Patankar, C. Spindloe, U. Chaulagain, K. M., J. Larour, R. L. Singh, R. Rodriguez, J. M. Gil, G. Espinosa, V. P., and C. Danson, "Counter-propagating radiative shock experiments on the Orion laser and the formation of radiative precursors," *High Energy Density Physics*, vol. 23, 2017.

[14] F. Suzuki-Vidal, T. Clayson, C. Stehlé, G. F. Swadling, J. M. Foster, J. Skidmore, P. Graham, G. C. Burdiak, S. V. Lebedev, U. Chaulagain, R. L. Singh, E. T. Gumbrell, S. Patankar, C. Spindloe, J. Larour, M. Kozlova, R. Rodriguez, J. M. Gil, G. Espinosa, P. Velarde, and C. Danson, "Counterpropagating Radiative Shock Experiments on the Orion Laser," *Physical Review Letters*, vol. 119, no. 055001, 2017.

[15] J. C. Bozier, G. Thiell, J. P. Le Breton, S. Azra, M. Decroisette, and D. Schirmann, "Experimental Observation of a Radiative Wave Generated in Xenon by a Laser-Driven Supercritical Shock," *Physics Review Letters*, vol. 57, no. 11, 1986.

[16] S. Bouquet, C. Stehlé, M. Koenig, J. P. Chièze, A. Benuzzi-Mounaix, D. Batani, S. Leygnac, X. Fleury, H. Merdji, C. Michaut, F. Thais, N. Grandjouan, T. Hall, E. Henry, V. Malka, and J. P. J. Lafon, "Observation of laser driven supercritical radiative shock precursors," *Physical Review Letters*, vol. 92, no. 22, 2004.

[17] M. Koenig, T. Vinci, A. Benuzzi-Mounaix, N. Ozaki, A. Ravasio, M. Rabec Le Glohaec, L. Boireau, C. Michaut, S. Bouquet, S. Atzeni, A. Schiavi, O. Peyrusse, and D. Batani, "Radiative shocks: An opportunity to study laboratory astrophysics," *Physics of Plasmas*, vol. 13, no. 056504, 2006.

[18] C. Stehlé, M. González, M. Kozlova, B. Rus, T. Mocek, O. Acef, J. P. Colombier, T. Lanz, N. Champion, K. Jakubczak, J. Polan, P. Barroso, D. Bauduin, E. Audit, J. Dostal, and M. Stupka, "Experimental study of radiative shocks at PALS facility," *Laser and Particle Beams*, vol. 28, jun 2010.

[19] A. Dizière, C. Michaut, M. Koenig, C. D. Gregory, A. Ravasio, Y. Sakawa, Y. Kuramitsu, T. Morita, T. Ide, H. Tanji, H. Takabe, P. Barroso, and J. M. Boudenne, "Highly radiative shock experiments driven by GEKKO XII," *Astrophysics and Space Science*, vol. 336, no. 1, 2011.

[20] R. P. Drake, F. W. Doss, R. G. McClarren, M. L. Adams, N. Amato, D. Bingham, C. C. Chou, C. DiStefano, K. Fidkowski, B. Fryxell, T. I. Gombosi, M. J. Grosskopf, J. P. Holloway, B. van der Holst, C. M. Huntington, S. Karni, C. M. Krauland, C. C. Kuranz, E. Larsen, B. van Leer, B. Mallick, D. Marion, W. Martin, J. E. Morel, E. S. Myra, V. Nair, K. G. Powell, L. Rauchwerger, P. Roe, E. Rutter, I. V. Sokolov, Q. Stout, B. R. Torralva, G. Toth, K. Thornton, and A. J. Visco, "Radiative effects

in radiative shocks in shock tubes," *High Energy Density Physics*, vol. 7, no. 3, 2011.

[21] R. Singh, C. Stehlé, F. Suzuki-Vidal, M. Kozlova, J. Larour, U. Chaulagain, T. Clayson, R. Rodriguez, J. Gil, J. Nejdl, M. Krus, J. Dostal, R. Dudzak, P. Barroso, O. Acef, M. Cotelo, and P. Velarde, "Experimental study of the interaction of two laser-driven radiative shocks at the PALS laser," *High Energy Density Physics*, vol. 23, jun 2017.

[22] G. C. Burdiak, S. V. Lebedev, R. P. Drake, A. J. Harvey-Thompson, G. F. Swadling, F. Suzuki-Vidal, J. Skidmore, L. Suttle, E. Khoory, L. Pickworth, P. de Grouchy, G. N. Hall, S. N. Bland, M. Weinwurm, and J. P. Chittenden, "The production and evolution of multiple converging radiative shock waves in gas-filled cylindrical liner z-pinch experiments," *High Energy Density Physics*, vol. 1, no. 9, 2013.

[23] G. C. Burdiak, S. V. Lebedev, A. J. Harvey-Thompson, G. F. Swadling, F. Suzuki-Vidal, G. N. Hall, E. Khoory, L. Pickworth, S. N. Bland, P. De Grouchy, J. Skidmore, L. Suttle, M. Bennett, N. P. L. Niasse, R. J. R. Williams, K. Blesener, L. Atoyan, A. Cahill, C. Hoyt, W. Potter, E. Rosenberg, P. Schrafel, and B. Kusse, "Radiative precursors driven by converging blast waves in noble gases," *Physics of Plasmas*, vol. 21, no. 033302, 2014.

[24] G. C. Burdiak, S. V. Lebedev, F. Suzuki-Vidal, G. F. Swadling, S. N. Bland, N. Niasse, L. Suttle, M. Bennet, J. Hare, M. Weinwurm, R. Rodriguez, J. Gil, and G. Espinosa, "Cylindrical liner Z-pinch experiments for fusion research and high-energy-density physics," *Journal of Plasma Physics*, vol. 81, no. 3, 2015.

[25] I. H. Mitchell, J. M. Bayley, J. P. Chittenden, J. F. Worley, a. E. Dangor, M. G. Haines, and P. Choi, "A high impedance mega-ampere generator for fiber z-pinch experiments," *Review of Scientific Instruments*, vol. 67, no. 4, 1996.

[26] Go-Araldite. http://www.go-araldite.com/products/epoxy-adhesives/araldite-instant-24ml-syringe. Accessed: 2017-09-14.

[27] G. F. Swadling, S. V. Lebedev, N. Niasse, J. P. Chittenden, G. N. Hall, F. Suzuki-Vidal, G. Burdiak, A. J. Harvey-Thompson, S. N. Bland, P. De Grouchy, E. Khoory, L. Pickworth, J. Skidmore, and L. Suttle, "Oblique shock structures formed during the ablation phase of aluminium wire array z-pinches," *Physics of Plasmas*, vol. 20, no. 022705, 2013.

[28] J. J. MacFarlane, I. E. Golovkin, and P. R. Woodruff, "HELIOS-CR - A 1-D radiation-magnetohydrodynamics code with inline atomic kinetics modeling," *Journal of Quantitative Spectroscopy and Radiative Transfer*, vol. 99, no. 1-3, 2006.

[29] D. D. Ryutov, "Characterizing the Plasmas of Z-Pinches," *IEEE Transactions on Plasma Science*, vol. 43, no. 8, 2015.

[30] A. Kramida, Yu. Ralchenko, J. Reader, and and NIST ASD Team. NIST Atomic Spectra Database (ver. 5.3), [Online]. Available: `http://physics.nist.gov/asd` [2016, October 20]. National Institute of Standards and Technology, Gaithersburg, MD., 2015.